Applied Catalysis B: Environmental 246 (2019) 296–302

Contents lists available at ScienceDirect

Applied Catalysis B: Environmental

journal homepage: www.elsevier.com/locate/apcatb

Review

Vertical nanosheet array of 1T phase MoS_2 for efficient and stable hydrogen evolution

Zhipeng Liu, Lei Zhao, Yuhua Liu, Zhichao Gao, Shisheng Yuan, Xiaotian Li, Nan Li*, Shiding Miao*

Key Laboratory of Automobile Materials (Ministry of Education), School of Materials Science and Engineering, Open Research Laboratory for Physicochemical Testing Methods of Functional Minerals (Ministry of Land and Resources), Jilin University, 2699 Qianjin Street, Changchun, 130012, PR China

ARTICLE INFO

Keywords:
Hydrogen evolution reaction
Efficient electrocatalysts
1T phase MoS_2
Self-supported structure
Vertical array

ABSTRACT

Metallic 1 T phase of molybdenum disulfide (1 T-phase MoS_2) was proposed as an more ideal electrocatalyst for the hydrogen evolution reaction (HER) than 2H-phase owing to its proliferated density of active sites and superior electroconductivity. Nevertheless, the conventional synthetic route of 1 T-phase MoS_2 through lithium intercalation suffers from tedious laboratory work and low yield, and the resulting powdery products are undesirable for practical applications. Herein, we developed a facile and scalable hydrothermal route to fabricate a self-supported electrode based on 1 T-phase MoS_2, which enables the 1 T-phase MoS_2 nanosheets to *in-situ* vertically grow on conductive carbon fiber cloth (1 T-MoS_2/CC). The resultant 1 T-MoS_2/CC combines advantages of the highly catalytically active phase of MoS_2 and the unique self-supported structure. MoS_2 nanosheets in 1 T-phase provide abundant active sites and high conductivity, while the self-supported structure endows the electrode with enhanced accessibility to active sites and efficient electron transfer throughout the structure. Owing to these merits, 1 T-MoS_2/CC delivered remarkable activity towards the HER with a small overpotential of 151 mV to afford 10 $mA{\cdot}cm^{-2}$ current density as well as brilliant stability, which is far superior to 2H-MoS_2/CC and its powdery counterpart (1 T-MoS_2). Therefore, this strategy makes the 1 T-MoS_2/CC a competitive electrocatalyst for hydrogen evolution.

1. Introduction

Hydrogen generation through electrochemical water splitting is one of the green chemistry tasks for sustainable energy production [1–3]. But the energy conversion efficiency is unsatisfactory due to the high operate potential and sluggish kinetics of the hydrogen evolution reaction (HER) and oxygen evolution reaction (OER) [4–6]. Accordingly, it is desired to develop electrocatalysts that can reduce the polarization potential and accelerate the reaction. Generally, noble metals (Pt and Pd) were considered as efficient catalysts, but practical application is hampered by their scarcity and cost-effect [7,8]. As a promising alternative, molybdenum disulfide (MoS_2) is receiving extensive attentions owing to its activity towards the HER, acid resistances and earth aboudant [9–11]. MoS_2 was typically synthesized in its thermodynamically stable polymorph of 2H-phase which occurs as a lamellar hexagonally packed structure with a Mo atom plane sandwiched between two symmetrical sulfur planes [12,13]. However, previous studies have confirmed that active sites in 2H-phase MoS_2 are limited in edges [14,15]. While the small proportion of edges and large inert basal planes will assuredly impede the HER performance [16,17]. In addition, 2H-phase MoS_2 is a type of semiconductors, and the low conductivity is a drawback to the electrocatalytic process [18].

Different from 2H phase, MoS_2 in 1 T phase occurs as an octahedral structure that is described as trigonal prism with one of the sulfur basal planes rotated by 60° around the *c*-axis [12,19]. This crystal structure renders MoS_2 metal-like conductivity and catalytically active basal plane towards the HER [20–22]. Hence 1 T-phase MoS_2 is proposed as a more ideal HER electrocatalysts than 2H-phase MoS_2 [23–25]. Nevertheless, 1 T-phase MoS_2 is conventionally synthesized by exfoliating bulk 2H-phase MoS_2 through a lithium intercalation/extraction route [26,27], which is undesirable for scaling up due to the following aspects: (1) the involved intercalating agent and intermediates are sensitive to water and oxygen, and the exfoliation process has to be carried out in a glove box; (2) the slow diffusion with respect to phase transformation of MoS_2 would always prolong the synthesis, and result in a low yield; (3) the powdery MoS_2 and the using of polymer binders to post-fabricate electrode would result in high contact resistance and blockage of active sites [28,29].

* Corresponding authors.
E-mail addresses: lin@jlu.edu.cn (N. Li), miaosd@iccas.ac.cn (S. Miao).

https://doi.org/10.1016/j.apcatb.2019.01.062
Received 25 June 2018; Received in revised form 14 January 2019; Accepted 19 January 2019
Available online 23 January 2019
0926-3373/

In response to these challenges, research efforts have been devoted to explore facile and more efficient ways to prepare the 1 T-phase MoS_2 and several "bottom-up" strategies including solvothermal/hydrothermal synthesis, colloidal synthesis and lithium molten salts method have been reported as feasible synthetic routes [29–33]. Compared to the lithium intercalation route, these methods do not use the inflammable agents, and products were obtained at a high yield, which is desirable for large-scale synthesis. However, further improvement in catalytic performance of the as-synthesized 1 T-phase MoS_2 is restricted by its powdery morphology. A promising option is to construct self-supported electrode by growing the 1 T-phase MoS_2 nanosheets directly on current-collecting substrate [34,35]. A self-supported structure is beneficial for electron transfer and mass transport, as well as preventing the blockage of active sites caused by binders [36,37]. With this in mind, we fabricated a self-supported hydrogen-evolving electrode based on 1 T-phase MoS_2 nanosheets. The electrode was constructed by *in-situ* vertically growing 1 T-phase MoS_2 nanosheets on a carbon fiber cloth (1 T-MoS_2/CC) via a facile and scalable hydrothermal method. The 1 T-phase MoS_2 in vertical array morphology provides abundant active sites and metal-like conductivity, while the self-supported structure can be served as cathods, and render the electrolyte more efficient accessible to the active sites. The carbon framework enables fast charge transfer, and therefore promotes the overall efficiency. On the basis of this features, the as-synthesized 1 T-MoS_2/CC exhibited remarkable performance with small overpotential, favorable kinetics and excellent electrochemical/air stability.

2. Experimental

2.1. Synthesis

To prepared the 1 T-MoS_2/CC self-supported electrode the 0.1 mmol ammonium molybdate ($Na_2MoO_4{\cdot}2H_2O$) and 0.5 mmol thiourea ($CS(NH_2)_2$) were dissolved in 15 mL mixture of water and propionic acid (volume ratio of 2:1). The mixture was stirred for 10 min to get a homogeneous solution, and then the solution was transferred into a 25 mL Teflon-lined stainless autoclave. A piece of carbon fiber cloth (2 cm × 3 cm), cleaned with 3 M HCl, deionized water and ethanol, was immersed in the solution. The autoclave was sealed and heated in an oven at 180 °C for 8 h. After cooling to room temperature, the carbon cloth was rinsed thoroughly with deionized water and ethanol for several times, and was dried in a vacuum at 60 °C. In a control experiment a 2H-MoS_2/CC self-supported electrode based on 2H-phase MoS_2 was synthesized with the same hydrothermal method at 220 °C for 24 h using pure water as a solvent. Powdery samples (1 T-MoS_2 and 2H-MoS_2) were also synthesized through the same procedure as that of 1 T-MoS_2/CC and 2H-MoS_2/CC with no addition of carbon cloth.

2.2. Characterization

Raman spectra were collected from a micro-Raman spectrometer (Renishaw) with a laser of 532 nm wavelength at 0.2 mW. The X-ray photoelectron spectroscopy (XPS) were obtained from a ESCALAB 250 electron spectrometer with an Al Kα radiation source ($h\nu$ = 1486.6 eV). DSC were conducted using a DSC-60 plus differential scanning calorimetry (SHIMADZU) with a heating rate of 5 °C/min in an argon atmosphere and the infrared spectra are obtained on a Fourier Transform infrared spectrometer (FT-IR) (NICOLET380. USA). The microstructure and morphology were observed under scanning electron microscopy (SEM, JEOL JSM-6700 F) and transmission electron microscopy (TEM, JEOL JEM-2100 F). The TEM samples were prepared by desquamating MoS_2 nanosheets from the carbon fibers through ultrasonic treatment.

2.3. Electrochemical measurements

Electrochemical test were carried out on a CHI 650E electrochemical workstation with a three electrode system in N_2-saturated 0.5 M H_2SO_4 or 1 M KOH aqueous solution. The 1 T-MoS_2/CC or 2H-MoS_2/CC (0.5 cm × 0.6 cm) was directly served as working electrode. The loading of MoS_2 on carbon cloth is calculated as 1.7 ± 0.2 $mg{\cdot}cm^{-2}$ according to the average value of additional mass on ten pieces of carbon cloth after hydrothermal synthesis. A graphite rod and a saturated $Hg/HgCl_2$ were served as the counter electrode and reference electrode, respectively. Powdery sample (1 T-MoS_2 or 2H-MoS_2) was dispersed in 1 mL of ethanol, along with 50 μL of Nafion solution (5 wt%) to prepare the catalyst ink. Afterwards, 5 μL of the catalyst ink was drop-cast onto the glassy carbon electrode to serve as the working electrode. Linear sweep voltammetry (LSV) measurements were scanned from 0 to -0.6 V vs RHE at a rate of 2 $mV{\cdot}s^{-1}$ after i-R correction. Tafel slopes were derived from their corresponding LSV data by fitting into the equation: $\eta = a + b{\cdot}\log j$. Cyclic votammetry (CV) measurements were conducted from 0.1 to 0.3 V vs RHE at a suite of scan rate ranging 20 ~ 100 $mV{\cdot}s^{-1}$ with 20 $mV{\cdot}s^{-1}$ interval to evaluate double-layer capacity. Chronoamperometry curve was recorded under a static overpotential of 200 mV vs. RHE to estimate the electrochemical stability. Electro impedance was recorded within frequencies ranging from 10 kHz to 0.01 Hz at a potential of 100 mV, and the impedance data were fitted to a simplified Randles circuit.

3. Result and discussion

3.1. Structure and morphology of the catalysts

The self-supported electrode of 1 T-phase MoS_2 nanosheet arrays on carbon fiber cloth (1 T-MoS_2/CC) was synthesized via a facile hydrothermal method. The hydrothermal environment was found to benefit the *in situ* growth of MoS_2 nanosheets, in which the carbon fibers act as nucleation and growth sites for MoS_2. Morphological and micro-structural characterizations of the as-synthesized 1 T-MoS_2/CC were performed by SEM and TEM. The SEM image (Fig. 1a) reveals that MoS_2 nanosheets are vertically oriented and uniformly distributed over the entire surface of carbon fibers, leaving substantial voids among them. Each individual nanosheet is 4–8 nm in thickness and approximately 100 nm in width, and the size of voids ranges from 50 to 200 nm. To get the TEM image (Fig. 1b) of 1 T-MoS_2, the nanosheets were ultrasonically peeled off from the fibers. Similar to the SEM observation the 1 T-MoS_2 nanosheets were found to consist of 5 to 10 layers, stacking together with an expanded interlayer distance of 0.68-0.8 nm (Fig. 1c). Rationally, the vertical array morphology and few-layered nanosheet structure is beneficial to provide abundant active sites to catalyze HER. In addition, substantial nanovoids allow sufficient accessibility for electrolyte and product.

3.2. Validation of 1 T phase MoS_2

A typical high resolution TEM (HRTEM) image from *c*-axis view (Fig. 1d) reveals that the basal planes of the nanosheets is composed of numerous crystalline nanodomains of ~5 nm. As shown in Fig. 1e and f, two distinct kinds of lattice can be identified from these domains, suggesting the coexistence of two types of polymorphs. The one with trigonal lattice corresponds to a crystal structure in an octahedral coordination (Fig. 1f, h) and therefore manifests the presence of 1 T phase. The other one with honeycomb-like lattice can be indexed to 2H phase, which consists of three Mo atoms and three overlapped S pairs arranged in a hexagon (Fig. 1e, g) [38,39]. The nanodomains assigned to 1 T-phase MoS_2 were dominant in numbers in the basal planes. In Fig. 1d domains of amorphous regions were also found, which might arise from the mismatch between 1 T phase and 2H phase. These amorphous regions contain substantial defects, and would probably provide additional catalytically active sites for HER. In order to make a clear comparison between 1 T-phase and 2H-phase MoS_2, we prepared 2H-MoS_2/CC as a reference sample through a similar hydrothermal method (see

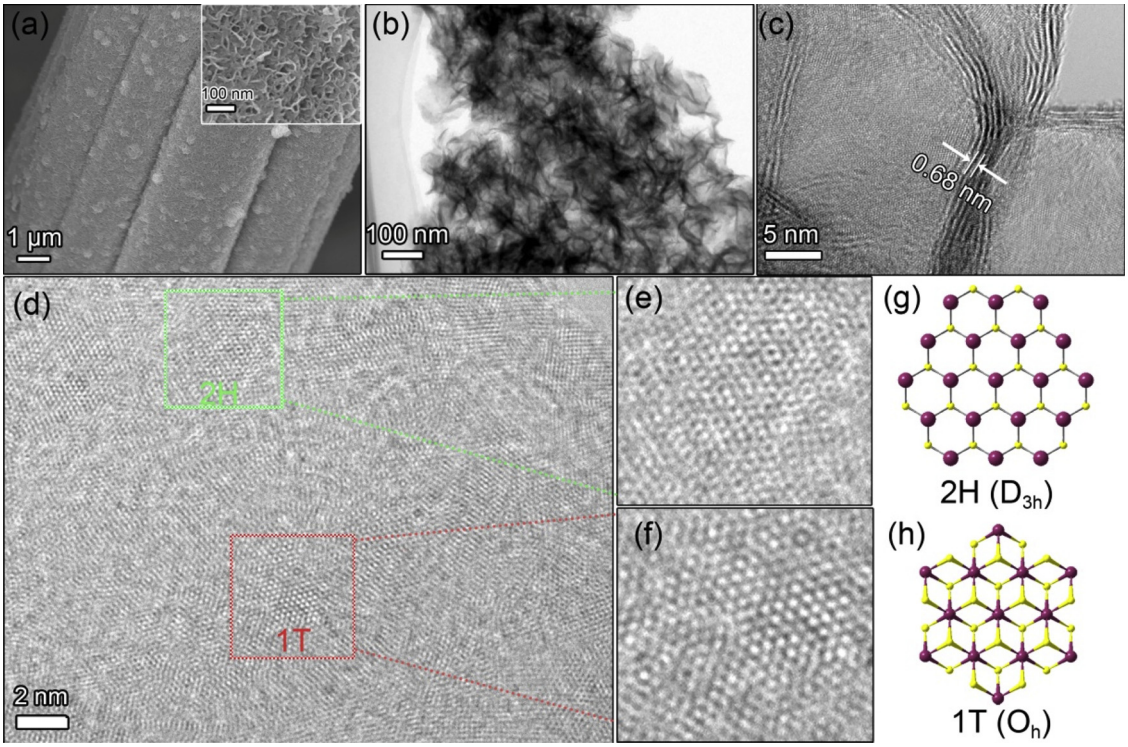

Fig. 1. (a) SEM images of 1 T-MoS_2/CC; (b–d) (HR)TEM images of MoS_2 nanosheets desquamated from 1 T-MoS_2/CC; (e, f) Zoom-in view of the selected area in d; (g, h) Illustration of structural configuration in 1 T- and 2H-phase MoS_2 from *c*-axis view.

experimental section). The corresponding SEM and TEM images in Fig. S1 of the supporting information (SI) suggest that 2H-MoS_2/CC electrode is of similar microscopic morphology as that of 1 T-MoS_2/CC. Actually, this vertical arrangement of MoS_2 is routinely obtained is hydrothermal synthesis [3]. However, essential difference in phase structure was observed. 2H-MoS_2/CC delivers almost perfect honeycomb-like lattices in its HRTEM images of basal plane (Fig. S1d), confirming this sample is composed of pure 2H-phase MoS_2.

Raman spectroscopy and X-ray photoelectron spectroscopy were used to identify the phasic and chemical compositions of the as-prepared self-supported electrodes. As shown in Fig. 2a, two notable bands at 381 and 404 cm^{-1} were found in both 1 T- and 2H-phases of MoS_2 which are attributed to E^1_{2g} and A_{1g} vibrational modes, respectively. The 1 T-MoS_2/CC exhibits three additional peaks at 146, 230 and 335 cm^{-1} which corresponds to J_1, J_2 and J_3 vibrational modes that occur only in 1 T-phase MoS_2 [40,41]. The successful synthesis of 1 T-phase MoS_2 in 1 T-MoS_2/CC was also confirmed by the XPS (Fig. 2b). The doublet of Mo 3d core-level spectra of 2H-MoS_2/CC can be precisely indexed to Mo^{4+} $3d_{3/2}$ and $3d_{5/2}$ of 2H-phase MoS_2, respectively. Comparing to that of 2H-MoS_2/CC, the doublet of 1 T-MoS_2/CC are asymmetric and broadened. A band shift towards lower binding energy was observed. These peaks can be deconvoluted into two doublets of XPS bands: one couple identical to the doublet in 2H-MoS_2/CC, and the other couple found at the lower binding energy. According to previous reports, the latter doublet correspond to Mo species in 1 T-phase MoS_2, which occurs as lower oxidative state relative to 2H-phase [21,27]. The S 2 P spectra gives similar results (Fig. S2 in the SI). In addition to peaks at 162.5 and 161.3 eV which can be assigned to 2H-phase MoS_2, the 1 T-MoS_2/CC exhibits two distinguish peaks at 161.7 and 160.5 eV, confirming the existence of 1 T-phase. Based on relative intensity of the representative peaks of 1 T-phase MoS_2 and 2H-phase MoS_2 we indicated the 1 T phase in sample 1 T-MoS_2/CC accounts for 72% in

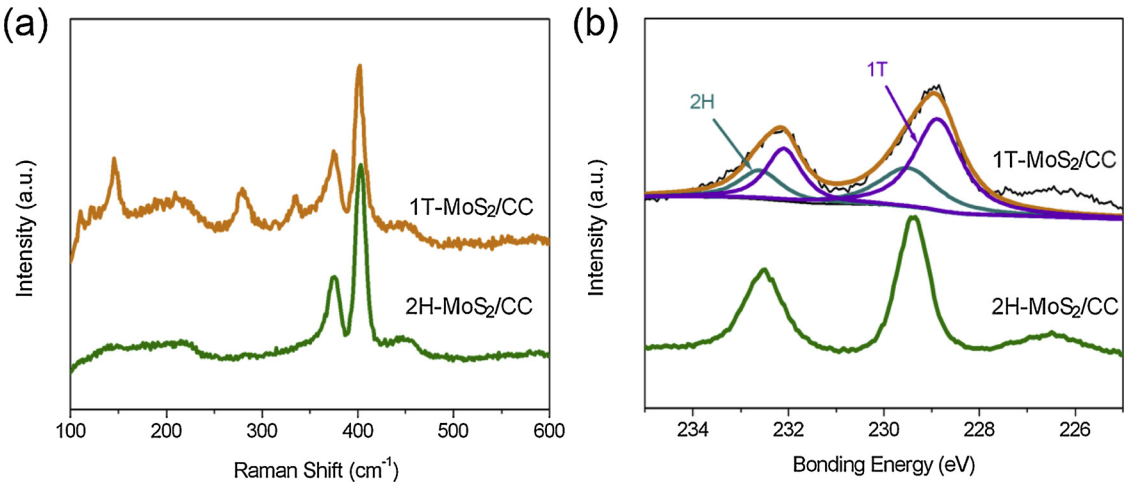

Fig. 2. (a) Raman spectra and (b) Mo 3d core-level XP spectra of 1 T-MoS_2/CC and 2H-MoS_2/CC.

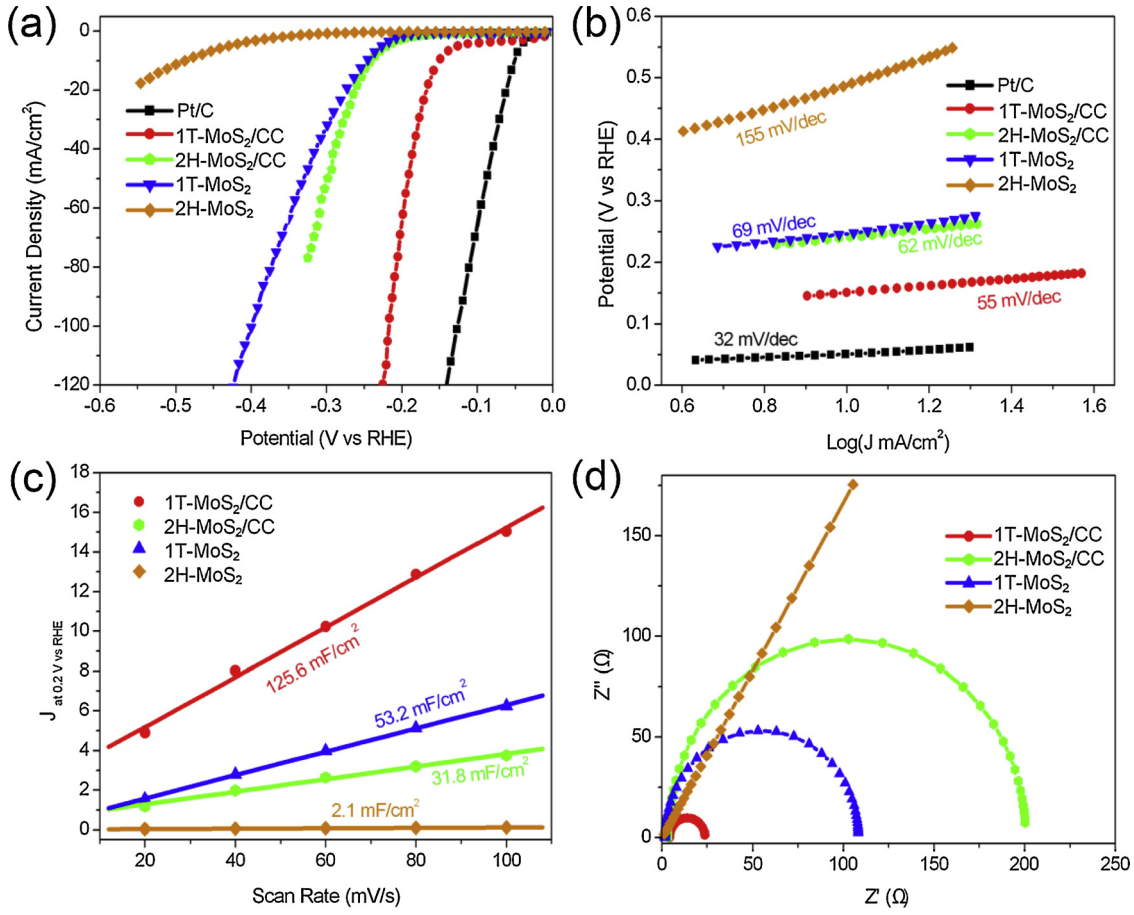

Fig. 3. The electrochemical performance of samples 1 T-MoS_2/CC, 2H-MoS_2/CC, powdery 1 T-MoS_2 and 2H-MoS_2: (a) LSV curves, (b) Tafel slopes, (c) linear regression of differences in current density ($J = J_a - J_b$) at 0.2 V plotted against the scan rate for the estimation of the effective surface area, and (d) electrochemical impedance spectroscopy Nyquist plots.

percentage. It is worth of noting that propionic acid is critical for the generation of 1 T-MoS_2 and only 2H-MoS_2 was obtained in pure water. This is probably related to the enhanced reducibility of thiourea in acid condition that results in Mo species in valence state lower than Mo(VI) (Fig. S3) and subsequently induces the formation of 1 T-MoS_2 [33].

3.3. HER activity of catalysts

The as-prepared 1 T-MoS_2/CC was directly used as working electrode for HER, and its electrocatalytic activity was evaluated by linear sweep voltammetry (LSV) measurement. For comparison, the commercial Pt/C (10%), 2H-MoS_2/CC, and powdery 1 T-MoS_2 and 2H-MoS_2 samples were also included. As depicted in Fig. 3a, our prepared 1 T-MoS_2/CC electrode shows outstanding activity towards the HER, and a small overpotential (η_{10}) of 151 mV was observed at the current density of 10 mA·cm^{-2}. This performance of 1 T-MoS_2/CC is obviously superior to that of 2H-MoS_2/CC. For example, the identical current density of 10 mA·cm^{-2} was not achieved until an overpotential of 226 mV was applied to the 2H-MoS_2/CC, which is 74 mV higher than 1 T-MoS_2/CC. The disparity in activity between 1 T-MoS_2/CC and 2H-MoS_2/CC becomes more prominent at high current density. Taking in consideration that both samples (1 T-MoS_2/CC and 2H-MoS_2/CC) are of similar vertical nanosheet morphology and self-supported architecture, the superior catalytic activity of 1 T-MoS_2/CC should stem from the intrinsic advantage of 1 T-phase. For the effect of self-supported structure, 1 T-MoS_2/CC was found to greatly surpass its powdery counterpart (1 T-MoS_2). To achieve a current density of 10 mA·cm^{-2}, 1 T-MoS_2 catalyst requires an overpotential of 247 mV which is almost 100 mV larger than 1 T-MoS_2/CC. Parameters of the HER catalyzed by the prepared materials were summarized in Table S1 which includes the over-potentials and Tafel slopes (see the SI). As aforementioned, the organic binders used in the fabrication of electrode are usually poor conductive and catalytically inert, which might block the active sites. Therefore, 1 T-MoS_2/CC self-supported catalyst was assumed to provide a large number of effective active sites and to facilitate the mass transport of electrolyte and product. In addition, the highly conductive carbon fiber framework in promotes electron transfer throughout the architecture and consequently enhances its electrocatalytic performance. This indication can be derived by the promoted performance observed in 2H-MoS_2/CC with respect to the powdery 2H-MoS_2, which can also be attributed to the self-supported structure. In addition, 1 T-MoS_2/CC also exhibits remarkable activity towards the HER in alkaline condition. (Fig. S4)

The Tafel slope of each sample was derived from the LSV curve to reflect its intrinsic reaction kinetics, wherein the result was found to follow the order: 1 T-MoS_2/CC < 2T-MoS_2/CC < 1 T-MoS_2 < 2T-MoS_2 (Fig. 3b). Generally, a smaller Tafel slope delivers a larger catalytic current density at lower overpotential, corresponding to more favorable kinetics. In the present work, except for Pt/C, our 1 T-MoS_2/CC exhibits the smallest Tafel slope, indicating their faster reaction rate over reference samples. It also demonstrates that the HER on this electrode proceeds by a Volmer-Heyrovsky mechanism, where a fast discharge of a proton is followed by a rate-limiting electrochemical desorption step.

3.4. Origin of the enhanced HER activity

To further elucidate the origin of the superior activity of 1 T-MoS_2/CC, the electrochemically active surface (ECSA) of each sample was

estimated based on its linear proportional relation with the corresponding double layer capacitance (C_{dl}) (Fig. 3c). As expected, 1 T-MoS_2/CC shows the largest C_{dl}, approximately three times as that of 2H-MoS_2/CC, suggesting more active sites available in 1 T-MoS_2/CC. The enlarged ECSA in 1 T-MoS_2/CC should predominantly arise from the proliferated catalytically active sites in the basal plane of 1 T-phase MoS_2. It is also worth of noting that the self-supported electrodes (1 T-MoS_2/CC and 2H-MoS_2/CC) exhibit substantially larger capacitance comparing with their powdery counterparts (1 T-MoS_2 and 2H-MoS_2) respectively, which is attributed to the high accessibility to active sites arising from the vertical orientated morphology and the avoidance of "binder-block-effect".

Moreover, the enhanced catalytic performance of 1 T-MoS_2/CC is associated with its high intrinsic conductivity. We conducted electrochemical impedance spectroscopic (EIS) measurements to investigate the electrode kinetics upon the HER. The Nyquist plots were presented in Figs. 3d and S5, where the diameters of the semicircles correlate with the charge transfer resistance (R_{ct}) at the solid-liquid interface. Obviously, samples constructed with 1 T-phase MoS_2 (1 T-MoS_2/CC and 1 T-MoS_2) display much smaller impedance than that with 2H-phase (2H-MoS_2/CC and 2H-MoS_2), in consistency with the higher intrinsic conductivity of 1 T-phase MoS_2. Actually, 1 T-phase MoS_2 exhibits a metal-like conducting feature, which electroconductivity is approximately six orders that of the semiconducting 2H one. This high conductivity can boost electron transfer through the nanosheets and lead to accelerated reaction rate. On the other hand, the self-supported electrodes (1 T-MoS_2/CC and 2H-MoS_2/CC) display smaller impedance relative to their powdery counterparts (1 T-MoS_2 and 2H-MoS_2) respectively, demonstrating that carbon fiber cloth with interconnected conductive network enables a fast charge transfer throughout the structure.

Based on the aforementioned results, the outstanding catalytic activity of 1 T-MoS_2/CC arises from the following aspects: a) 1 T-phase MoS_2 with active basal plane and metal-like conducting feature provides abundant active sites and high conductivity; b) the self-supported structure free from "binder-block-effect" ensures efficient access to active sites, and the highly conductive carbon fiber framework facilitates the electron transfer throughout the electrode. The synergistic effect of 1 T-phase of MoS_2 and the self-supported structure enables 1 T-MoS_2/CC as a highly active HER electrocatalyst.

3.5. Stability of the catalysts

Stability is also a requisite factor for a competitive electrocatalyst. In contrast to 2H MoS_2, 1 T-phase MoS_2 is metastable in thermodynamic, which may lead to performance degradation. Therefore, we conducted chronoamperometry measurement to evaluate the electrochemical stability of 1 T-MoS_2/CC. As depicted in Fig. 4a, 1 T-MoS_2/CC delivers almost constant current density under stationary overpotential. After 20 h of electrochemical catalysis, approximately 98% of the current density is retained and the vertical nanosheet arrays were well preserved (see the SEM images of Fig. S6 in the SI). Moreover, the LSV curve recorded after 5000 cycles of CV tests repeats well with the fresh prepared one (Fig. 4b). All these results reveal the excellent electrochemical stability of 1 T-MoS_2/CC. In addition, 1 T-MoS_2/CC exhibits remarkable air stability. An experiment was conducted by exposing the 1 T-MoS_2/CC to air for 45 days before it was used for the HER catalysis. The LSV curve of which coincides well with its original counterpart with negligible activity decay (Fig. 4c). The sample was also characterized by the Raman spectrometry, and it exhibits a similar Raman bands as the original one, confirming 1 T-phase of MoS_2 in the self-supported electrode is rather stable in air (Fig. 4d). However, 1 T-phase MoS_2 prepared via the previous n-butyl lithium intercalation/extraction approach cannot sustain in air for 45 days [42,43].

As a step further, we inspected thermal stability of 1 T-MoS_2/CC. Firstly, it was annealed at 150 °C under Ar flow for 2 h. At such high temperature, the conversional 1 T-MoS_2 obtained via chemical exfoliation route is expected to undergo a conversion reaction towards the thermodynamically stable 2H-MoS_2 [44,45]. Nevertheless, the concentration of 1 T polymorph of MoS_2 in the as-synthesized 1 T-MoS_2/CC is almost identical to the original one (Fig. S7a). Consequently, the catalytic activity of 1 T-MoS_2/CC is well retained after annealing (Fig. S7b). To further reveal the remarkable thermal stability of 1 T-MoS_2/CC, differential scanning calorimetry (DSC) was conducted and the corresponding curves are depicted in Fig. 5a. A similar self-supported electrode constructed with 1 T-MoS_2 synthesized via hydrothermal method according to a previous report was also included as a reference sample (denoted as reference-1 T-MoS_2/CC, see Fig S8 for structural information) [29]. In contrast to the featureless 2H-MoS_2/CC, our 1 T-MoS_2/CC exhibits a predominant exothermic peak at about 239 °C, corresponding to the conversion reaction from 1 T phase to 2H phase. Notably, the identical conversion reaction is routinely occurs at 95 °C for 1 T-MoS_2 obtained through Li exfoliation route and thus the thermal stability of 1 T-MoS_2/CC is substantially enhanced [46,47]. Moreover, this conversion temperature is 90 °C higher than that for the reference 1 T-MoS_2/CC. The superior thermal stability of 1 T-MoS_2/CC comparing with the reference sample is attributed to the distinct generation condition. The reference 1 T-MoS_2/CC is obtained in pure water, whereas the 1 T-MoS_2/CC in this work is fabricated with the presence of propionic acid. Propionic acid as an organic agent can adhere on the MoS_2 nanosheets and contribute to the stability. For validation, the corresponding powdery samples (1 T-MoS_2, 2H-MoS_2 and reference 1 T-MoS_2) are investigated by infrared spectrum (IR). As displayed in Fig. 5b, infrared-absorption bands that are indexed to CH_3- or CH_2- (2907, 2842 cm^{-1}), C=O (1720 cm^{-1}) and C–O (1236 cm^{-1}) appear only in the pattern of 1 T-MoS_2, revealing that some organic functional groups are absrobed on the nanosheets. Actually, previous work have demonstrated that functional group adsorption and covalent functionalization with organic agent including acetic acid group is favorable for the stability of metallic MoS_2 [48,49]. Therefore, we propose that these adherent groups are probably the origin of the superior electrochemical/thermal stability of 1 T-MoS_2/CC in this work.

4. Conclusion

In conclusion, a self-supported electrocatalyst has been successfully prepared with vertical nanosheet array of 1 T-phase MoS_2 on carbon cloth through a facile hydrothermal method. The self-supported structure was investigated as an electrode for the HER. The 1 T-phase of MoS_2 provides proliferated active sites and high conductivity, and the self-supported structure endows the electrode with enhanced accessibility to active sites and efficient charge transfer. The combination of 1 T phase MoS_2 and the self-supported structure enables 1 T-MoS_2/CC with remarkable activity towards the HER with a small overpotential of 151 mV at a current destiny of 10 $mA{\cdot}cm^{-2}$ and favorable Tafel slope of 55 $mV{\cdot}dec^{-1}$. Furthermore, 1 T-MoS_2/CC performs excellent electrochemical and thermal stability. These properties enable 1 T-MoS_2/CC a highly competitive candidate for high-performance and low-cost HER electrocatalysts.

Funding sources

This study was supported by the National Natural Science Foundation of China (21673097) and Jilin Province/Jilin University Co-construction Project – Funds for New Materials (SXGJSF2017-3).

Notes

The authors declare no competing financial interest.

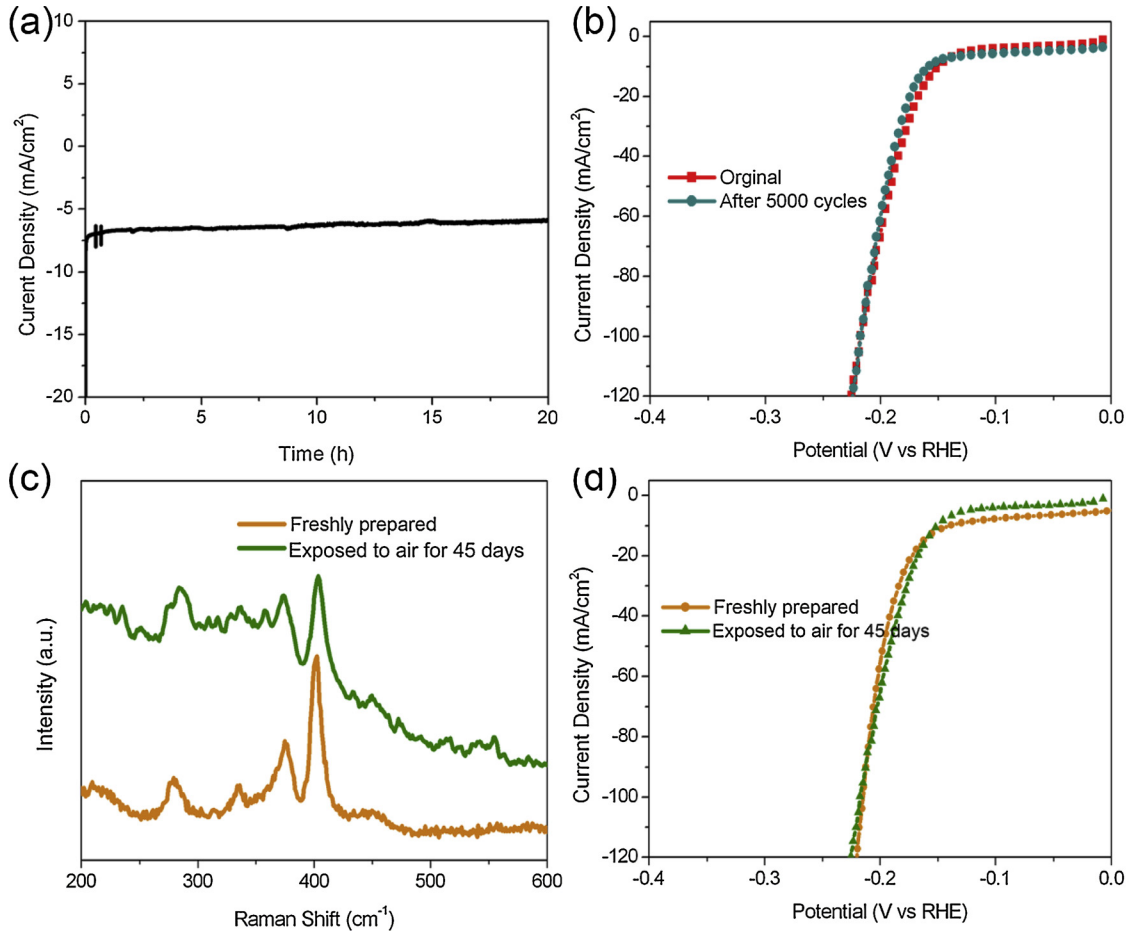

Fig. 4. (a) The chronoamperometry profile of 1 T-MoS_2/CC at the overpotential of 100 mV; (b) LSV curves of the fresh prepared sample and that after 5000 cycles of CV tests; (c) Raman shift of the 1 T-MoS_2/CC and that exposed to air for 45 days; and (d) the corresponding LSV curves.

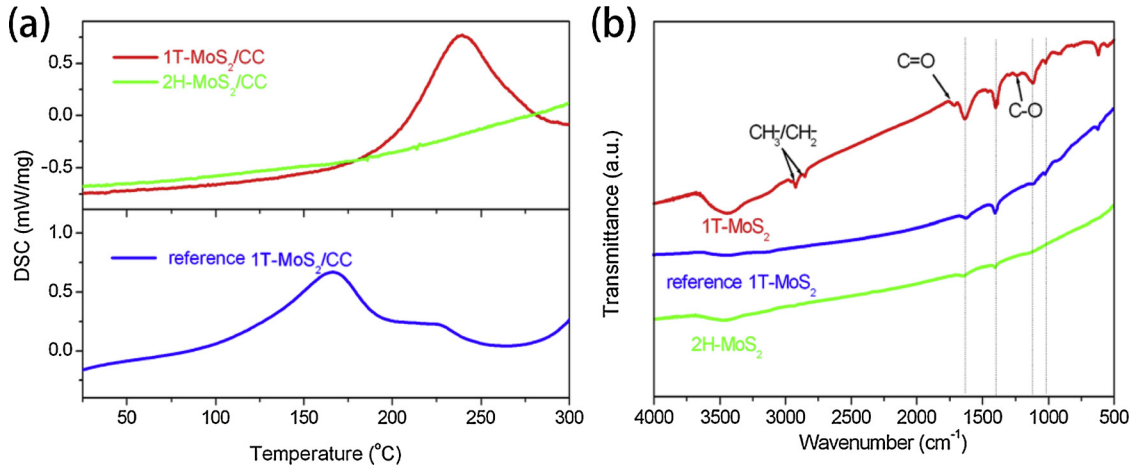

Fig. 5. (a) DSC curves of 1 T-MoS_2/CC, 2H-MoS_2/CC and reference 1 T-MoS_2/CC; (b) IR spectra of the corresponding powdery samples.

Appendix A. Supplementary data

Supplementary material related to this article can be found, in the online version, at doi:https://doi.org/10.1016/j.apcatb.2019.01.062.

References

[1] D. Merki, X. Hu, Energy Environ. Sci. 4 (2011) 3878.
[2] Y. Okamoto, S. Ida, J. Hyodo, H. Hagiwara, T. Ishihara, J. Am. Chem. Soc. 133 (2011) 18034–18037.
[3] X.X. Zou, Y. Zhang, Chem. Soc. Rev. 44 (2015) 5148–5180.
[4] Y. Shi, B. Zhang, Chem. Soc. Rev. 45 (2016) 1529–1541.
[5] C.C. McCrory, S. Jung, I.M. Ferrer, S.M. Chatman, J.C. Peters, T.F. Jaramillo, J. Am. Chem. Soc. 137 (2015) 4347–4357.
[6] W. Zhang, W.Z. Lai, R. Cao, Chem. Rev. 117 (2017) 3717–3797.
[7] M.A. Abbas, J.H. Bang, Chem. Mater. 27 (2015) 7218–7235.
[8] J. Hu, C.X. Zhang, X.Y. Meng, H. Lin, C. Hu, X. Long, S.H. Yang, J. Mater. Chem. A 5 (2017) 5995–6012.
[9] M. Cai, F. Zhang, C. Zhang, C.B. Lu, Y.F. He, Y. Qu, H. Tian, X.L. Feng, X.D. Zhuang, J. Mater. Chem. A 6 (2018) 138–144.
[10] S.Q. Su, Q.W. Zhou, Z.Q. Zeng, D. Hu, X. Wang, M.L. Jin, X.S. Gao, R. Notzel, G.F. Zhou, Z. Zhang, J.M. Liu, ACS Appl. Mater. Interfaces 10 (2018) 8026–8035.

[11] S. Bellani, L. Najafi, A. Capasso, A.E.D. Castillo, M.R. Antognazza, F. Bonaccorso, J. Mater. Chem. A 5 (2017) 4384–4396.
[12] M. Chhowalla, H.S. Shin, G. Eda, L.J. Li, K.P. Loh, H. Zhang, Nat. Chem. 5 (2013) 263–275.
[13] Y. Yan, B. Xia, Z. Xu, X. Wang, ACS Catal. 4 (2014) 1693–1705.
[14] T.F. Jaramillo, K.P. Jørgensen, J. Bonde, J.H. Nielsen, S. Horch, I. Chorkendorff, Science 317 (2007) 100–102.
[15] B. Hinnemann, P.G. Moses, J. Bonde, K.P. Jørgensen, J.H. Nielsen, S. Horch, I. Chorkendorff, J.K. Nørskov, J. Am. Chem. Soc. 127 (2005) 5308–5309.
[16] J.B. Ding, Y. Zhou, Y.G. Li, S.J. Guo, X.Q. Huang, Chem. Mater. 28 (2016) 2074–2080.
[17] J. Xie, J. Zhang, S. Li, F. Grote, X. Zhang, H. Zhang, R. Wang, Y. Lei, B. Pan, Y. Xie, J. Am. Chem. Soc. 135 (2013) 17881–17888.
[18] Q.H. Wang, K. Kalantar-Zadeh, A. Kis, J.N. Coleman, M.S. Strano, Nat. Nanotechnol. 7 (2012) 699–712.
[19] Y.C. Lin, D.O. Dumcenco, Y.S. Huang, K. Suenaga, Nat. Nanotechnol. 9 (2014) 391–396.
[20] R. Kappera, D. Voiry, S.E. Yalcin, B. Branch, G. Gupta, A.D. Mohite, M. Chhowalla, Nat. Mater. 13 (2014) 1128–1134.
[21] D. Voiry, M. Salehi, R. Silva, T. Fujita, M. Chen, T. Asefa, V.B. Shenoy, G. Eda, M. Chhowalla, Nano Lett. 13 (2013) 6222–6227.
[22] M.A. Lukowski, A.S. Daniel, F. Meng, A. Forticaux, L. Li, S. Jin, J. Am. Chem. Soc. 135 (2013) 10274–10277.
[23] Q. Tang, D.E. Jiang, ACS Catal. 6 (2016) 4953–4961.
[24] C.L. Tan, Z.M. Luo, A. Chaturvedi, Y.Q. Cai, Y.H. Du, Y. Gong, Y. Huang, Z.C. Lai, X. Zhang, L.R. Zheng, X.Y. Qi, M.H. Goh, J. Wang, S.K. Han, X.J. Wu, L. Gu, C. Kloc, H. Zhang, Adv. Mater. 30 (2018) 1705509.
[25] Y. Yin, J.C. Han, Y.M. Zhang, X.H. Zhang, P. Xu, Q. Yuan, L. Samad, X.J. Wang, Y. Wang, Z.H. Zhang, P. Zhang, X.Z. Cao, B. Song, S. Jin, J. Am. Chem. Soc. 138 (2016) 7965–7972.
[26] G. Eda, H. Yamaguchi, D. Voiry, T. Fujita, M. Chen, M. Chhowalla, Nano Lett. 11 (2011) 5111–5116.
[27] M. Acerce, D. Voiry, M. Chhowalla, Nat. Nanotechnol. 10 (2015) 313–318.
[28] J. Zheng, H. Zhang, S. Dong, Y. Liu, C. Tai Nai, H. Suk Shin, H. Young Jeong, B. Liu, K. Ping Loh, Nat. Commun. 5 (2014) 2995.
[29] X. Geng, W. Sun, W. Wu, B. Chen, A. Al-Hilo, M. Benamara, H. Zhu, F. Watanabe, J. Cui, T.P. Chen, Nat. Commun. 7 (2016) 10672.
[30] Q. Liu, X. Li, Q. He, A. Khalil, D. Liu, T. Xiang, X. Wu, L. Song, Small 11 (2015) 5556–5564.
[31] B. Mahler, V. Hoepfner, K. Liao, G.A. Ozin, J. Am. Chem. Soc. 136 (2014) 14121–14127.
[32] K. Chang, X. Hai, H. Pang, H. Zhang, L. Shi, G. Liu, H. Liu, G. Zhao, M. Li, J. Ye, Adv. Mater. 28 (2016) 10033–10041.
[33] Z.P. Liu, Z.C. Gao, Y.H. Liu, M.S. Xia, R.W. Wang, N. Li, ACS Appl. Mater. Interfaces 9 (2017) 25291–25297.
[34] A.Y. Lu, X. Yang, C.C. Tseng, S. Min, S.H. Lin, C.L. Hsu, H. Li, H. Idriss, J.L. Kuo, K.W. Huang, L.J. Li, Small 12 (2016) 5530–5537.
[35] J.M. Cao, J. Zhou, Y.F. Zhang, Y.X. Wang, X.W. Liu, ACS Appl. Mater. Interfaces 10 (2018) 1752–1760.
[36] J. Wang, F. Xu, H. Jin, Y. Chen, Y. Wang, Adv. Mater. 29 (2017) 1605838.
[37] M.Y. Wang, X.T. Yu, Z. Wang, X.Z. Gong, Z.C. Guo, L. Dai, J. Mater. Chem. A 5 (2017) 9488–9513.
[38] P. Cheng, K. Sun, Y.H. Hu, Nano Lett. 16 (2016) 572–576.
[39] L. Cai, J. He, Q. Liu, T. Yao, L. Chen, W. Yan, F. Hu, Y. Jiang, Y. Zhao, T. Hu, Z. Sun, S. Wei, J. Am. Chem. Soc. 137 (2015) 2622–2627.
[40] R. Lv, J.A. Robinson, R.E. Schaak, D. Sun, Y.F. Sun, T.E. Mallouk, M. Terrones, Acc. Chem. Res. 48 (2015) 56–64.
[41] Y.Q. Fang, J. Pan, J.Q. He, R.C. Luo, D. Wang, X.L. Che, K.J. Bu, W. Zhao, P. Liu, G. Mu, H. Zhang, T.Q. Lin, F.Q. Huang, Angew. Chem. Int. Ed. 57 (2018) 1232–1235.
[42] S. Jiménez Sandoval, D. Yang, R.F. Frindt, J.C. Irwin, Phys. Rev. B 44 (1991) 3955–3962.
[43] M. Calandra, Phys. Rev. B 88 (2013) 245428.
[44] Q. Tang, D.E. Jiang, Chem. Mater. 27 (2015) 3743–3748.
[45] F. Wypych, R. Schollhor, J. Chem. Soc. Chem. Commun. 19 (1992) 1386.
[46] A.S. Goloveshkin, I.S. Bushmarinov, A.A. Korlyukov, M.I. Buzin, V.I. Zaikovskii, N.D. Lenenko, A.S. Golub, Langmuir 31 (2015) 8953–8960.
[47] A.S. Goloveshkin, I.S. Bushmarinov, N.D. Lenenko, M.I. Buzin, A.S. Golub, M.Y. Antipin, J. Phys. Chem. C 117 (2013) 8509–8515.
[48] J.I. Paredes, J.M. Munuera, S. Villar-Rodil, L. Guardia, M. Ayan-Varela, A. Pagan, S.D. Aznar-Cervantes, J.L. Cenis, A. Martinez-Alonso, J.M.D. Tascon, ACS Appl. Mater. Interfaces 8 (2016) 27974–27986.
[49] J. Heising, M.G. Kanatzidis, J. Am. Chem. Soc. 121 (1999) 11720–11732.